*Sirte University Scientific Journal (Applied Sciences)* *Vol. 7 (2), 53–75, December 2017*

# Influence of Anodizing Conditions on The Mechanical Properties of Anodic Alumina Films Fabricated in Sulphuric Acid

*Ali K. M. Al-zenati*[*1]

***E-mail: alikmz@yahoo.co.uk***

[1]*Department of Mechanical, Faculty of Engineering, Sirte University, Sirte, Libya*

## Abstract

The hardness and elastic modulus for the anodic films formed on high purity aluminium are investigated by nano-indentation and micro-hardness techniques. Micro-hardness investigation is revealed that the film hardness reduces as the distance increases from aluminium/film interface due to the chemical degradation in the outer region of the film during anodizing process, which increases with rise of the anodizing time and temperature. Moreover nano-indentation is shown that the hardness and elastic modulus for hard films are relatively independent of the selected anodizing conditions, with respective values of ~ 5.6 ± 0.40 GPa and ~ 110.8 ± 6 GPa. However, for films fabricated at 20 C°, the hardness and elastic modulus increases linearly with rise of current density and with reduction of anodizing time. This reduction of hardness and elastic modulus with increased anodizing time indicates the role of chemical degradation which is promoted by increased temperature.

**Keywords:** *Anodizing, Anodic alumina film, Mechanical properties.*

## 1. Introduction

Porous anodic films can be achieved by anodizing of metals such as aluminium, magnesium[1], titanium[2-4], tantalum[5-8], tungsten[9], zirconium[10-11], iron[12-13] and their alloys[14]. Porous anodic films formed on aluminium can provide protection against corrosion and wear giving a good adhesive[15-18] for paint. These anodic porous films utilize for nanotechnologies because of their sub-micron and ordered pores[19-22]. The anodic oxide films show that their properties are largely dependent of anodizing conditions such as current density, anodizing time, electrolyte and its temperature[23-25].These factors have been widely researched in recent years[26-28]. A lot of investigations were carried out in the area of anodic

oxidation of aluminium ever since its first industrial utilization[29-30]. Nanoindentation technique has proven itself to be an extremely useful for testing material at microscale. This technique gives accurate comparison for determination of the properties of in-situ matrix constituents with the same materials in their bulk[31-33]. Nanoindentation test provides precise measure values for hardness and elastic modulus simultaneously[34-37]. The nanoindentation technique is suitable method for determination of hardness of anodic films and it is possible to measure the hardness at various locations through the depth of the films. The hardness of anodic oxide films are usually very high, unlike thin anodic oxides are influenced by the hardness of the metal substrate itself. The metal substrate can not be protected by the anodic oxide films from high pressure but, they can provide a good resistance of surface scratch. The hardness of the anodic oxide films is dependent of the anodizing conditions i.e. it raises as the electrolyte concentration, its temperature or aggression decrease. The anodic oxide films produced by d.c. current have higher hardness; in contrast with those fabricated by a.c. current which have lower hardness. The hardness of the anodic oxide films differ throughout their depth[38], namely the hardest layer is adjacent to the metal substrate and decreases toward the film surfaces as temperature rises. The hardness throughout the film thickness is inversely proportional to the film porosity. It is very significant to control hard anodizing conditions; otherwise the high increase in concentration, temperature or current density can lead to the rise of the electrolyte solubility which produces powdery or spongy outer layer of the anodic oxide film. The hardness of materials can be obtained by Brinell, Vickers and Rockwell methods, scratch methods or the Martens method. However, these methods are not convenient for hardness measurements of anodic oxide films because they do not take into account variations in hardness. This difficulty to measure hardness with depth for thin films can be achieved by nano-indentation technique immediately or by micro-hardness technique with specific procedures; measurements achieve on cross-section of the anodized specimen for determination of hardness with depth throughout the anodic oxide film as done in this present study.

## 2. Experimental Work

### Specimen Preparation

Specimens of high purity aluminium “99.99 %” of size 2 x 3 $cm^2$. The samples were subjected to electropolishing process for 3 minutes at constant voltage of 20 V in a 60 % perchloric

acid/ethanol electrolyte [20 : 80 % by volume] at 10 C° which produced a mirror-finish. Following electropolishing, the specimens were washed immediately in ethanol, followed by rinsing in deionised water and final drying by a cool air stream. Before the anodizing process, the working area of the specimens [1 x 2 $cm^2$] was defined by masking the specimen edges with lacquer [Stopper 45 Mac Dermid]. Each specimen was connected by an insulated aluminium rod via clips to the positive terminal of power supply.

## Anodizing Process

Specimens of electropolishing high purity aluminium were individually anodized in 24.5 wt % sulphuric acid at selected constant current densities [10, 20 and 30 $mA/cm^2$] for a constant anodizing time of 5400 s and under 30 $mA/cm^2$ for various anodizing time for 1000, 3000 and 4000 s at 0 and 20 C° in two-electrode, glass cell with a cylindrical sheet of high purity aluminium foil [8 x 22 $cm^2$] was connected to the negative terminal of power supply, acting as a cathode while the specimen was connected to the positive terminal of a d.c. power, functioning as an anode in order to investigate the mechanical properties of the resultant anodic films.

## Specimen Examination

## Micro-hardness Measurements

The micro-hardness technique is an electromechanical instrument for determination of the hardness of materials. The tester utilizes a Vickers indenter, which is programmed into the tester's firmware.

The test is achieved by the following steps:

-The diamond indenter is forced into the surface of material utilizing a fixed known load force.

-The length of the diagonals of the resulting indent in the tested material surface is measured to determine the resistance of the material to penetration.

The diagonal length is then converted into a hardness number on Vickers scale [HV] which is calculated according to:

$$HV = 1.000 * 10^3 * P / A_s = 2.000 * 10^3 [P \sin(\alpha/2) / d^2] = 1.8544 [p / d^2]$$

Where, $HV$ is the Vickers hardness number.

$P$ is the test force in (kgf),

$A_s$ is the surface area of indent (mm),

$d$ is the mean diagonal of indent (mm) and

$\alpha$ is the face angle of indenter and equal to 136˚.

The unit of the Vickers hardness number normally used Newtons rather than g-force or kg-force, therefore the equation:

$HV = 0.0018544[p / d^2]$

Where, 0.1891 is a constant related to the geometry of the indenter,
$P$ is the test load (N) and $d$ is the mean diagonal of indent (mm).

## Preparation of Specimens for Micro-hardness Test

The specimen strip is fixed into a capsule filling with resin, normal to its surface for examination in cross-section. The resin is a mixture of Araldite hardener and Araldite resin [1 : 10 % by weight]. The capsule then left over night to dry. The cross-section of specimen was finished by mechanical polishing with silicon carbide grade (800 to 1200) following by diamond polishing in stages from (6 to 2 to 0.25 μ) respectively. The indents were made across the alumina thickness along a line at an angle of about 45˚ to aluminium/film interface, with at least 5 times the indent diameter between each indent, see figure (1).

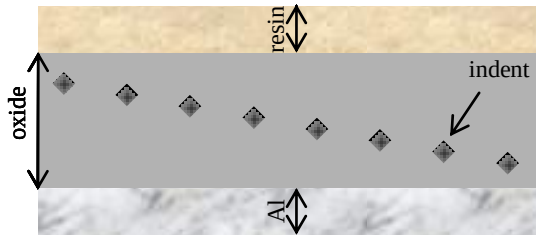


Figure (1). Schematic diagram of the indents utilized to determine the hardness on a cross-section of a porous anodic alumina film by micro-hardness technique.

## Instrumented Indentation Testing (IIT)

The hardness (H) and elastic modulus (E) of very thin films, coatings and surface layers can be measured by IIT from the load-displacement transients, using the Oliver and Pharr method with a Beckovich indenter.

Measurement of hardness (H) can be obtained by the following equation:

$H=P/A$

Where, $P$ is the load applied to specimen surface and $A$ is the projected contact area of the indenter at such a load.

The elastic modulus (E) is determined from the reduced modulus ($E_r$) as follows:

$E_r = \sqrt{\pi}. S/2\beta\sqrt{A}$

where, $S$ is unloading stiffness and $\beta$ is a constant which depends only on the geometry of the indenter.

$1/E_r = (1–v^2)/E + (1+v_i^2)/E_i$

Where, v is the poisson's ratio for the test material (0.22), $E_i$ and vi are the elastic modulus and poisson's ratio respectively of the indenter. The elastic constant ($E_i$ = 1141 GPa) and poisson's ratio ($v_i$ = 0.07) for diamond indenter.

## Preparation of Specimen for IIT Test

Specimen (1 x 1 $cm^2$) mounted with double contact glue onto the sample holder e.g. aluminium bar. Software program provide pre-selected positions of indentations number on the surface of the anodic alumina film with a penetration depth of 2 μm or less depending on the film thickness of the indenter. The tests were achieved at variable displacements in order to determine the properties as function of changing substrate effects. For utilizing the Berkovich indenter, the distance between indents should be at least 20 to 30 times of the maximum penetration depth. To avoid effects of aluminium substrate, the depth of indent was selected to be less than 10 % of oxide thickness, see figure (2).

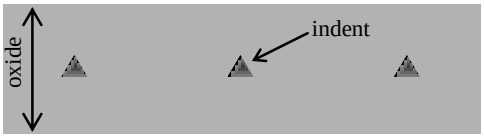


Figure (2). Schematic diagram of the indents utilized to determine the hardness and elastic modulus on a surface of a porous anodic alumina film by nano-indentation technique.

## 3. Results

Anodizing of the aluminium thicken the air-formed film producing thick anodic porous film which have a good resistance to wear and corrosion of the aluminium surface enabling widespread applications even in nanotechnological industries such as magnetic, electronic and optoelectronic devices i.e. capacitors. This study utilizes nanoindentation and microhardness, with particular interest to reveal the effect of anodizing conditions such as current density, anodizing time and temperature of electrolyte on the hardness of the alumina oxides. Nanoindentation tests were achieved on the film surfaces, with a maximum depth of indentation of 2 μm. Micro-hardness tests were obtained on cross-section of the anodic films at various locations through the thickness of the films.

### Microhardness tests on cross-section of anodic alumina films grown at 0 C°

Measurements of microhardness were carried out on cross-sections of anodic films formed on high purity aluminium in 24.5 wt % sulphuric acid for different current densities i.e. 10, 20 and 30 mA/cm$^2$, for constant anodizing time, 5400 s at 0 C° as shown in figures (3) to (5). Moreover, tests were obtained on the anodic films fabricated under the same temperature but for various times, i.e. 1000, 3000 and 4000 s at 30 mA/cm$^2$ as seen in figures (6) to (8). Figures (3) to (8) reveal that the reduction in hardness of the anodic alumina films increases from aluminium/film interface to film/air interface as determined in the table (1). The percentage of hardness reduction across the film thickness is determined using hardness values measured near the aluminium/film interface and near the film/air interface.

Table 1. Results of micro-hardness tests were obtained on cross-sections of alumina films formed at 0 C°

| Current density ($mA/cm^2$) | Anodizing time (s) | Load (g) | Film thickness (μm) | Reduction of hardness % |
|---|---|---|---|---|
| 10 | 5400 | 25 | 30.4 ± 0.87 | 6 |
| 20 | 5400 | 100 | 63.8 ± 1.71 | 10 |
| 30 | 5400 | 100 | 100.5 ± 2.02 | 13 |
| 30 | 4000 | 100 | 75.2 ± 1.58 | 11 |
| 30 | 3000 | 100 | 53.9 ± 1.30 | 7 |
| 30 | 1000 | 25 | 18.7 ± 0.47 | 5 |

.The hardness reduction between the aluminium substrate to the film surface increases from 5 to 13 % as anodizing time raises i.e. 1000, 3000, 4000 and 5400 s for oxide films formed at 30 $mA/cm^2$ as revealed in table (1) and figures (6) to (8).

## Microhardness tests on cross-section of anodic alumina films grown at 20 C°

Tests of microhardness were achieved on cross-sections of alumina films formed in 24.5 wt % sulphuric acid at 20 C° for various current densities i.e. 10, 20 and 30 $mA/cm^2$ for constant anodizing time, 5400 s, see figures (3) to (5). Tests were also obtained on cross-section of anodic alumina films fabricated in 24.5 wt % sulphuric acid at 20 C° for different anodizing times, namely 1000, 3000 and 4000 s under constant current density, 30 $mA/cm^2$ as presented in figures (6) to (8). Generally, the reduction of hardness between aluminium/film interface and film/air interface is much greater from 12 to 38 % for films grown at 20 C° in comparison with those (5 to 13 %) formed at 0 C°. As anodizing time increases i.e. 1000, 3000, 4000 and 5400 s the reduction of the hardness for oxide films formed at 30 $mA/cm^2$ rises from 12 to 34 % as revealed in table (2) and figures (6) to (8).

Table 2. Results of micro-hardness tests were obtained on cross-sections of alumina films formed at 20 C˚.

| Current density ($mA/cm^2$) | Anodizing time (s) | Load (g) | Film thickness (μm) | Reduction of hardness % |
|---|---|---|---|---|
| 10 | 5400 | 25 | 27.8 ± 1.4 | 31 |
| 20 | 5400 | 25 | 55.2 ± 2.6 | 38 |
| 30 | 5400 | 100 | 86.8 ± 3.21 | 34 |
| 30 | 4000 | 100 | 65.4 ± 1.95 | 20 |
| 30 | 3000 | 25 | 51.3 ± 1.24 | 17 |
| 30 | 1000 | 10 | 16.7 ± 0.19 | 12 |

Figure (3) shows the hardness at approximately 2 μm distance from aluminium substrate for films fabricated at 10 $mA/cm^2$ for 5400 s, but at various temperature (0 and 20 C˚). The hardness increases by 15 % for anodic alumina film grown at 0 C˚ compared with that for alumina film formed at 20 C˚ as in table (3). Generally, the hardness of anodic oxide film fabricated at 0 C˚ is approximately constant until about 12 μm distance from aluminium/film interface and then reduces slightly by 6 % towards the film/air interface. However, a large reduction in the hardness can be seen obviously for anodic alumina films formed at 20 C˚ with increased distance from the aluminium/film interface to the film/air interface. The hardness is decreased near the oxide surface by 31 % relative to that near the aluminium substrate surface. The hardness is roughly steady for films fabricated under 20 $mA/cm^2$ and at 0 C˚. In contrast, the hardness reduces steeply from aluminium/film interface to film surface formed at 20 C˚ as seen in figure (4). The reduction of hardness with increased distance from aluminium/film interface for anodic alumina film formed at 30 $mA/cm^2$ at 0 C˚ for 5400 s is lower (13 %) than that of the film grown under the same anodizing conditions but at different temperature 20 C˚ (34 %), see tables (1), (2) and figure (5).

Table 3. Percentage of hardness reduction at approximately 2 μm from aluminum substrate on cross-sections of alumina films formed at 0 and 20 C˚.

| Current density ($mA/cm^2$) | Anodizing time (s) | Hardness (HV) close to Al (~ 2 μm) at 0 C˚ | Hardness (HV) close to Al (~ 2 μm) at 20 C˚ | Reduction of hardness at (~ 2 μm) % |
|---|---|---|---|---|
| 10 | 5400 | 420.7 | 358.1 | 15 |
| 20 | 5400 | 410.1 | 371.5 | 9 |
| 30 | 5400 | 402.3 | 375.1 | 7 |
| 30 | 4000 | 411.9 | 377.5 | 8 |
| 30 | 3000 | 409.3 | 389.4 | 5 |
| 30 | 1000 | 421.9 | 369.4 | 12 |

The values of hardness at the aluminium/film interface and at the film/air interface as in tables (4) and (5).

Table 4. The values of film hardness measured close to Al substrate and close to film surface at 0 C˚.

| Current density ($mA/cm^2$) | Anodizing time (s) | Distance from Al/film interface (μm) | Hardness (HV) close to Al | Distance from Al/film interface (μm) | Hardness (HV) close to film surface |
|---|---|---|---|---|---|
| 10 | 5400 | 2.21 | 420.7 | 28.12 | 394.1 |
| 20 | 5400 | 2.56 | 410.1 | 60.9 | 371.1 |
| 30 | 5400 | 2.33 | 402.3 | 94.81 | 350.5 |
| 30 | 4000 | 2.41 | 411.9 | 68.59 | 368.4 |
| 30 | 3000 | 2.30 | 409.3 | 51.14 | 380.3 |
| 30 | 1000 | 2.15 | 421.9 | 15.98 | 399.2 |

Table 5. The values of film hardness measured close to Al substrate and close to film surface at 20 C˚.

| Current density ($mA/cm^2$) | Anodizing time (s) | Distance from Al/film interface (μm) | Hardness (HV) close to Al | Distance from Al/film interface (μm) | Hardness (HV) close to film surface |
|---|---|---|---|---|---|
| 10 | 5400 | 2.10 | 358.1 | 24.10 | 246.9 |
| 20 | 5400 | 2.21 | 371.5 | 52.95 | 231.7 |
| 30 | 5400 | 2.40 | 375.1 | 83.14 | 248.3 |
| 30 | 4000 | 2.08 | 377.5 | 62.30 | 303.4 |
| 30 | 3000 | 2.54 | 389.4 | 45.11 | 321.6 |
| 30 | 1000 | 2.23 | 369.4 | 14.05 | 326.1 |

Tables (6) and (7) reveal the hardness values in HV close to film surface that change to IS unit (GPa), for films fabricated at 0 C˚ the hardness reports low values in comparison with values of nano-indentation in table (8). The hardness also shows reduction with rise of anodizing time for films formed at 30 $mA/cm^2$ and, for both temperatures (0 and 20 C˚).

Table 6. The values of HV hardness close to film surface converted into IS units (GPa) for alumina films formed at 0 C˚.

| Current density ($mA/cm^2$) | Anodizing time (s) | Distance from Al/film interface (μm) | Hardness (HV) close to film surface | Hardness (GPa)x(HV 0.009807) |
|---|---|---|---|---|
| 10 | 5400 | 28.12 | 394.1 | 3.865 |
| 20 | 5400 | 60.9 | 371.1 | 3.639 |
| 30 | 5400 | 94.81 | 350.5 | 3.437 |
| 30 | 4000 | 68.59 | 368.4 | 3.613 |

| | | | | |
|---|---|---|---|---|
| 30 | 3000 | 51.14 | 380.3 | 3.730 |
| 30 | 1000 | 15.98 | 399.2 | 3.915 |

Table 7). The values of HV hardness close to film surface converted into IS units (GPa) for alumina films formed at 20 C˚.

| Current density ($mA/cm^2$) | Anodizing time (s) | Distance from Al/film interface (μm) | Hardness (HV) close to film surface | Hardness (GPa)x(HV 0.009807) |
|---|---|---|---|---|
| 10 | 5400 | 24.10 | 246.9 | 2.421 |
| 20 | 5400 | 52.95 | 231.7 | 2.272 |
| 30 | 5400 | 83.14 | 248.3 | 2.435 |
| 30 | 4000 | 62.30 | 303.4 | 2.975 |
| 30 | 3000 | 45.11 | 321.6 | 3.154 |
| 30 | 1000 | 14.05 | 326.1 | 3.198 |

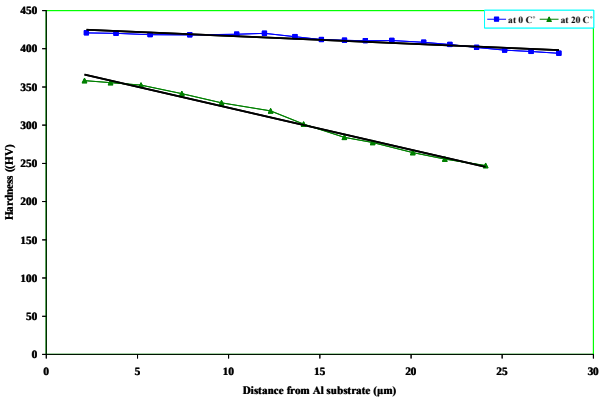


Figure(3). Microhardness through a cross section of an anodic alumina film fabricated at 10 $mA/cm^2$ for 5400 s in 24.5 wt % sulphuric acid at 0 and 20 C˚.

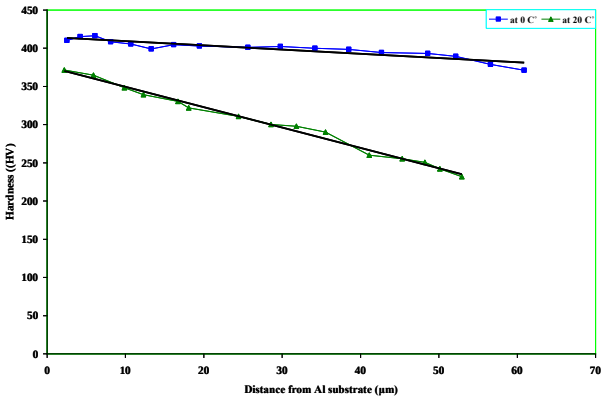


Figure(4). Microhardness through a cross section of an anodic alumina film fabricated at 20 $mA/cm^2$ for 5400 s in 24.5 wt % sulphuric acid at 0 and 20 C˚.

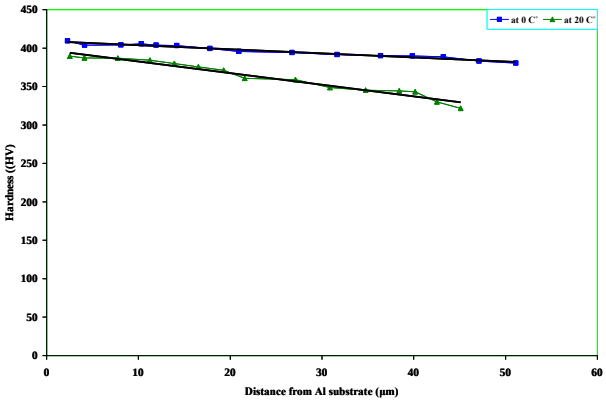


Figure(7). Microhardness through a cross section of an anodic alumina film fabricated at 30 mA/cm$^2$ for 3000 s in 24.5 wt % sulphuric acid at 0 and 20 C˚.

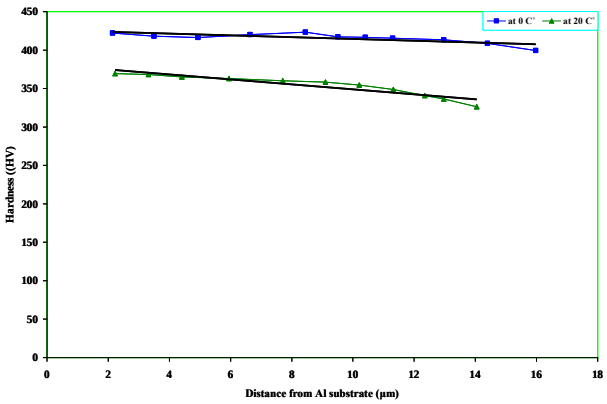


Figure(8). Microhardness through a cross section of an anodic alumina film fabricated at 30 mA/cm$^2$ for 1000 s in 24.5 wt % sulphuric acid at 0 and 20 C˚.

## Nano-indentation Tests on The Anodic Alumina Surface

Nano-indentation determines the hardness and elastic modulus under a constant depth of 2000 nm on the surface of porous anodic alumina film formed at 10, 20 mA/cm$^2$ for constant time of 5400 s and at 30 mA/cm$^2$ for various times i.e. 1000, 3000, 4000 and 5400 s at 0 and 20 C˚.

To avoid interaction with deformed material around the previous indent, the indents were chosen to be separated from each other by at least more than 5 times the diameter of the indent. The effect of the aluminium substrate must be avoided by determining the depth of the indenter less than 10 % of the thickness of tested films.

The elastic recovery ($E_c$) can be calculated as follows:

$E_c = h_{max} - h_f$

Where, $E_c$ is the elastic recovery,

$h_{max}$ is the maximum depth of the impression, when the load reaches the maximum value and

$h_f$ is the final depth of the indent, when the load reaches zero.

The ratio of elastic recovery[39-40] can be determined by the following equation:

The ratio of elastic recovery = $h_f / h_{max}$

Tables (8) and (9) reveal the mean hardness, mean elastic modulus and minimum-maximum load for the whole cycles of the tested films. Figures (9) and (10) show the hardness and elastic modulus values of the alumina films formed on aluminium substrate at 10, 20 and 30 mA/cm$^2$ for a constant time 5400 s at 0 C˚, roughly constant at ~ 5.6 ± 0.40 GPa and ~ 110.8 ± 6 GPa respectively. However, the trend of hardness and elastic modulus for films formed under the same anodizing conditions but at 20 C˚ increases nearly linearly as current density rises as seen in figures (9) and (10).

Table 8. The mean hardness, the mean elastic modulus and the minimum-maximum load for specimens anodized at 0 C˚

| Current density (mA/cm$^2$) | Anodizing time(s) | Mean hardness (GPa) | Mean elastic modulus (GPa) | Minimum-maximum load (mN) |
|---|---|---|---|---|
| 10 | 5400 | 5.44 ± 0.2 | 109.90 ± 3.8 | 385-415 |
| 20 | 5400 | 5.60 ± 0.4 | 110.90 ± 4.8 | 201-238 |
| 30 | 5400 | 5.67 ± 0.6 | 111.74 ± 9.9 | 351-479 |
| 30 | 4000 | 6.03 ± 0.5 | 115.76 ± 9.1 | 347-455 |
| 30 | 3000 | 5.20 ± 0.4 | 103.86 ± 6.0 | 332-390 |
| 30 | 1000 | 5.57 ± 0.2 | 109.88 ± 4.8 | 353-417 |

Table 9. The mean hardness, the mean elastic modulus and the minimum-maximum load for specimens anodized at 20 C˚.

| Current density (mA/cm$^2$) | Anodizing time(s) | Mean hardness (GPa) | Mean elastic modulus (GPa) | Minimum-maximum load (mN) |
|---|---|---|---|---|
| 10 | 5400 | 1.71 ± 0.02 | 53.34 ± 0.44 | 165-180 |
| 20 | 5400 | 2.22 ± 0.06 | 59.03 ± 1.04 | 152-161 |

| | | | | |
|---|---|---|---|---|
| 30 | 5400 | 2.79 ± 0.08 | 63.22 ± 1.50 | 171-182 |
| 30 | 4000 | 3.50 ± 0.18 | 81.02 ± 2.1 | 249-273 |
| 30 | 3000 | 4.03 ± 0.14 | 88.98 ± 2.23 | 299-315 |
| 30 | 1000 | 4.83 ± 0.06 | 100.81 ± 1.04 | 337-348 |

The influence of the anodizing time on the hardness of films fabricated under current density of 30 mA/cm$^2$ for 1000, 3000, 4000 and 5400 s at 0 C˚. The hardness reduces by 7 % for film grown at 3000 s in comparison with that fabricated at 1000 s. It then increases by 14 % for film formed for 4000 s. lastly, the hardness decreases by 6 % at film grown for 5400 s. The average of hardness for films formed at 30 mA/cm$^2$ for various anodizing times is ~ 5.6 ± 0.43 GPa, see figure (11).

As seen from figure (12) the elastic modulus affected by anodizing time at 0 C˚, where the modulus reduces by 5 % for film formed at 3000 s as compared with film fabricated for 1000 s. The elastic modulus increases by 10 % for film achieved for 4000 s in comparison with that grown at 3000 s. Finally, the elastic modulus value reduces approximately by 3 % for film fabricated for 5400 s.

Figure (11) shows the reduction of hardness for films formed at 30 mA/cm$^2$ for different anodizing times namely 3000, 4000 and 5400 s at 20 C˚ is higher by 17 %, 28 % and 42 % respectively compared with that fabricated for 1000 s. Figure (12) reveals that the trend of elastic modulus for the same films gives approximately the same trend behaviour of hardness.

The mean standard deviation of hardness and elastic modulus of films fabricated at 0 C˚ is 77 % and 78 % respectively higher than those of films formed at 20 C˚. High roughness and low homogeneity of the hard films and existence of flaws might be response for this high value of deviation.

Tables (8) and (9) reveal the influence of temperature on mechanical properties of the outer region of the films. Hardness and elastic modulus reduce as temperature of anodizing electrolyte rises which is in agreement with previous results[41]. The hardness and elastic modulus of anodic film grown at 10 mA/cm$^2$ at 20 C˚ for 5400 s reduce by 69 % and 51 %

Table 10. The hardness, elastic modulus, maximum load, elastic recovery, elastic ratio, creep deformation and time of creep achieved from the first and fifteenth cycles of nano-indentation for alumina films fabricated at 0 C˚

| Number of cycle | Current density ($mA/cm^2$) | Anodizing time (s) | Maximum load (mN) | Hardness (GPa) | Elastic modulus (GPa) | Elastic recovery (nm) | Creep deformation (nm) | Time of creep (s) | Ratio of elastic |
|---|---|---|---|---|---|---|---|---|---|
| 1 | 10 | 5400 | 397.3 | 5.4 | 112.9 | 475.5 | 81.7 | 11.6 | 0.77 |
| 15 | 10 | 5400 | 378.2 | 4.5 | 104.2 | 469.1 | 88.2 | 11.4 | 0.78 |
| 1 | 20 | 5400 | 202.2 | 4.2 | 109.3 | 479.1 | 83.1 | 11.4 | 0.77 |
| 15 | 20 | 5400 | 221.9 | 4.4 | 111.9 | 492.2 | 87.3 | 11.4 | 0.77 |
| 1 | 30 | 5400 | 392.9 | 5.1 | 104.1 | 507.9 | 79.8 | 11.6 | 0.76 |
| 15 | 30 | 5400 | 390.5 | 5.3 | 106.8 | 474.2 | 87.8 | 11.8 | 0.77 |
| 1 | 30 | 4000 | 407.7 | 5.8 | 112.3 | 482.4 | 69.3 | 11.4 | 0.76 |
| 15 | 30 | 4000 | 426.4 | 5.2 | 109.1 | 509.1 | 73.5 | 11.4 | 0.76 |
| 1 | 30 | 3000 | 350.7 | 4.8 | 105.6 | 509.4 | 85.3 | 11.4 | 0.76 |
| 15 | 30 | 3000 | 366.1 | 4.9 | 104.7 | 531.8 | 102.2 | 11.7 | 0.75 |
| 1 | 30 | 1000 | 379.5 | 5.3 | 109.2 | 508.7 | 94.6 | 11.7 | 0.76 |
| 15 | 30 | 1000 | 368.9 | 4.7 | 104.7 | 510.3 | 73.9 | 11.2 | 0.76 |

respectively compared with those of film fabricated under the same anodizing conditions but at 0 C˚. For film formed at 20 $mA/cm^2$ for 5400 s at 0 C˚ the hardness and elastic modulus increase by 60 % and 47 % respectively in comparison with film grown at 20 $mA/cm^2$ for 5400 s at 20 C˚. Moreover, respective reductions 51 % and 43 % were determined the hardness and elastic modulus for films formed at 30 $mA/cm^2$ for 5400 s at 20 C˚ compared with those of film fabricated at 30 $mA/cm^2$ at 0 C˚ for the same anodizing time.

The hardness and elastic modulus, maximum load, elastic recovery, elastic ratio, creep deformation and time creep were achieved from the first and fifteenth cycles “tests” of indentation for films fabricated at 10 and 20 $mA/cm^2$ for 5400 s and at 30 $mA/cm^2$ for 1000, 3000, 4000 and 5400 s at 0 and 20 C˚ as seen in tables (10) and (11).

.

Table 11. The hardness, elastic modulus, maximum load, elastic recovery, elastic ratio, creep deformation and time of creep achieved from the first and fifteenth cycles of nano-indentation for alumina films fabricated at 20 C.˚

| Number of cycle | Current density ($mA/cm^2$) | Anodizing time (s) | Maximum load (mN) | Hardness (GPa) | Elastic modulus (GPa) | Elastic recovery (nm) | Creep deformation (nm) | Time of creep (s) | Ratio of elastic |
|---|---|---|---|---|---|---|---|---|---|
| 1 | 10 | 5400 | 183.1 | 2.1 | 52.3 | 322.7 | 79.1 | 10.8 | 0.84 |
| 15 | 10 | 5400 | 176.4 | 2.0 | 52.7 | 304.5 | 70.2 | 10.7 | 0.85 |
| 1 | 20 | 5400 | 155.6 | 2.2 | 53.9 | 558.8 | 87.3 | 10.3 | 0.76 |
| 15 | 20 | 5400 | 159.1 | 2.3 | 54.9 | 570.1 | 101.1 | 12.3 | 0.75 |
| 1 | 30 | 5400 | 176.1 | 2.5 | 57.1 | 479.9 | 104.5 | 11.7 | 0.78 |
| 15 | 30 | 5400 | 179.6 | 2.4 | 56.9 | 462.5 | 87.6 | 11.7 | 0.79 |
| 1 | 30 | 4000 | 253.1 | 3.4 | 75.8 | 484.7 | 102.3 | 11.3 | 0.78 |
| 15 | 30 | 4000 | 267.1 | 3.5 | 77.1 | 478.4 | 109.7 | 13.5 | 0.78 |
| 1 | 30 | 3000 | 306.5 | 4.1 | 89.2 | 499.8 | 91.4 | 11.5 | 0.77 |
| 15 | 30 | 3000 | 307.7 | 3.7 | 83.5 | 487.1 | 104.6 | 12.6 | 0.78 |
| 1 | 30 | 1000 | 347.1 | 4.5 | 96.4 | 506.7 | 90.0 | 10.4 | 0.76 |
| 15 | 30 | 1000 | 351.4 | 4.7 | 97.5 | 512.1 | 86.5 | 10.2 | 0.76 |

Time of creep and ratio of elastic give roughly the same trend for both films fabricated at 0 and 20 C˚. However, the creep deformation reports low values for films formed at 0 C˚. Approximately similar behavior for the whole films can be seen by the load-displacement transients which is achieved by nano-indentation technique; in contrast variations only happen in the load that is dependant of the hardness, and in the slope of unloading curve which is related to the extent of the creep and the elastic response of the film material as in figures (13)-(16). Figures (17)-(20) show that the load-time responses consist of three regions; the peak region is the creep which occurs for 10-12 s, the first and last portions represent the loading and unloading regions respectively.

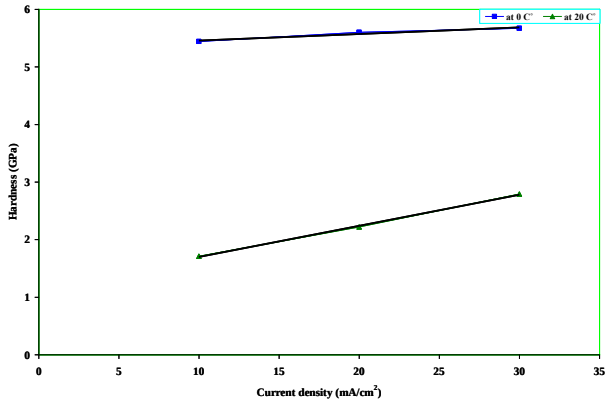


Figure(9). Hardness versus current density for anodic alumina films formed in 24.5 wt % sulphuric acid for 5400 s at 0 and 20 C˚.

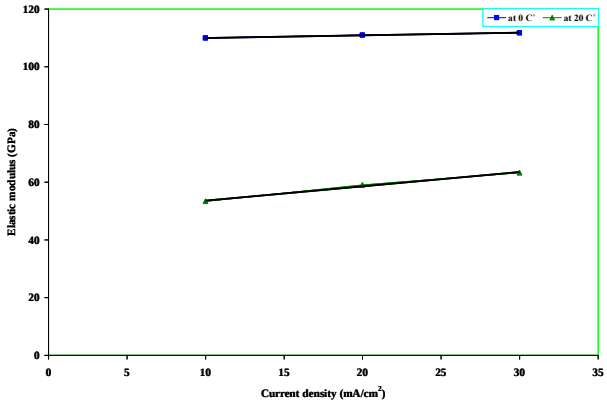


Figure(10). Elastic modulus versus current density for anodic alumina films formed in 24.5 wt % sulphuric acid for 5400 s at 0 and 20 C˚.

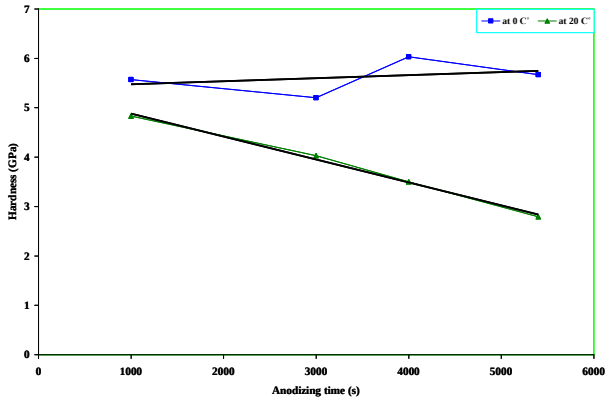


Figure(11). Hardness versus anodizing time for anodic alumina films formed at 30 mA/cm$^2$ in 24.5 wt % sulphuric acid at 0 and 20 C˚.

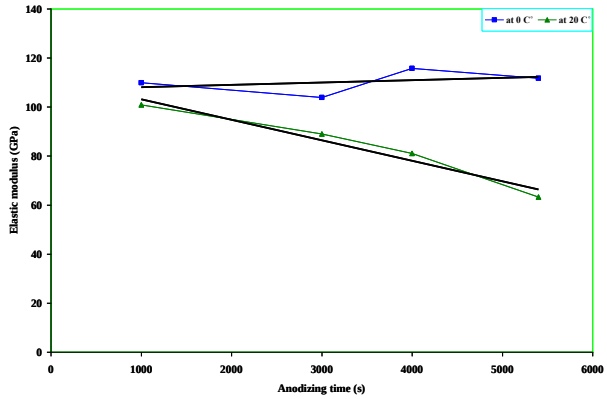


Figure(12). Elastic modulus versus anodizing time for anodic alumina films formed at 30 mA/cm$^2$ in 24.5 wt % sulphuric acid at 0 and 20 C˚.

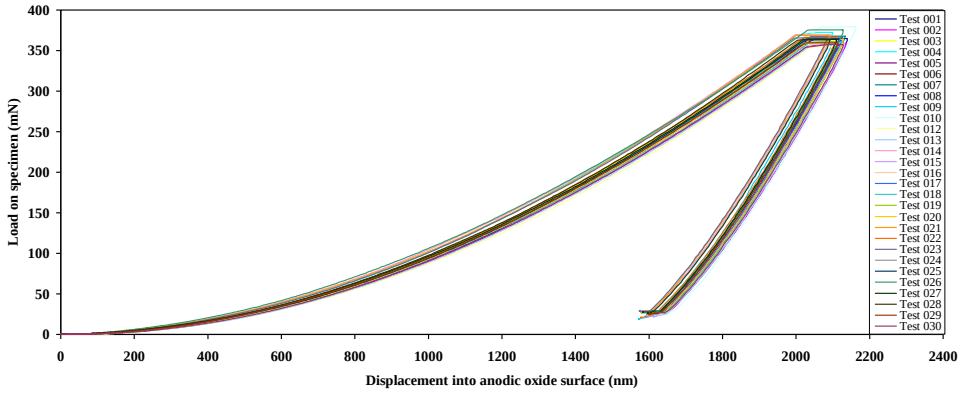


Figure (13). Load on spcimen-displacement into anodic oxide surface for several indents by nanoindention with depth about 2000 nm into film formed at 10 mA/cm$^2$ for 5400 s at 0 C˚.

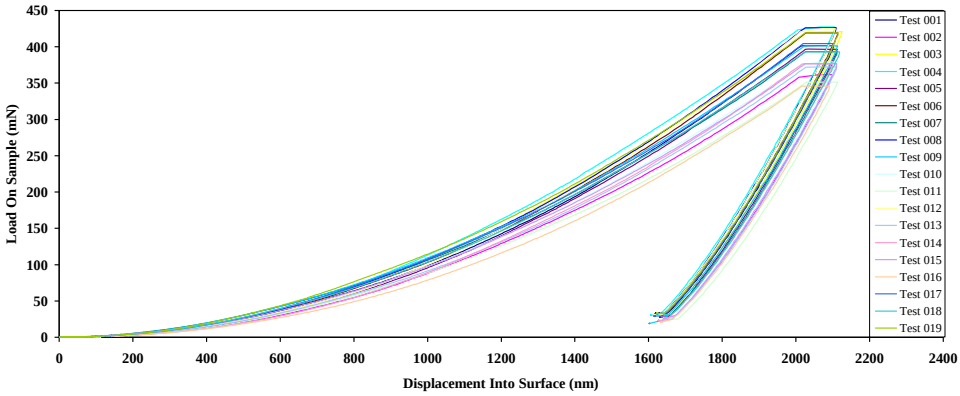


Figure (14). Load on spcimen-displacement into anodic oxide surface for several indents by nanoindention with depth about 2000 nm into film formed at 30 mA/cm$^2$ for 5400 s at 0 C˚.

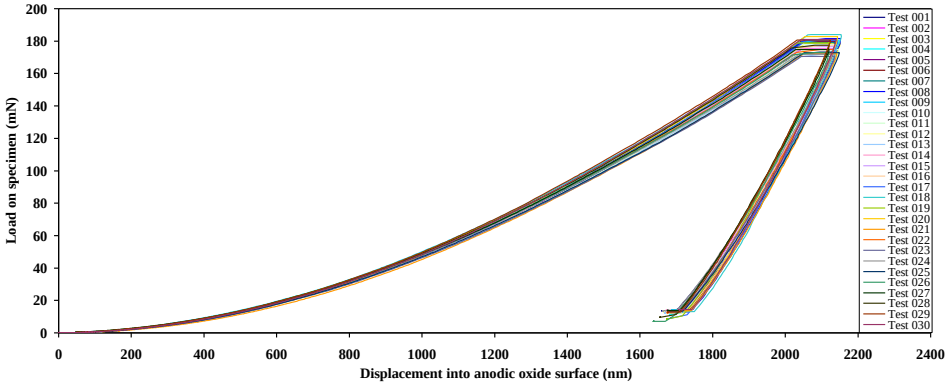


Figure (16). Load on spcimen-displacement into anodic oxide surface for several indents by nanoindention with depth about 2000 nm into film formed at 30 mA/cm$^2$ for 5400 s at 20 C˚.

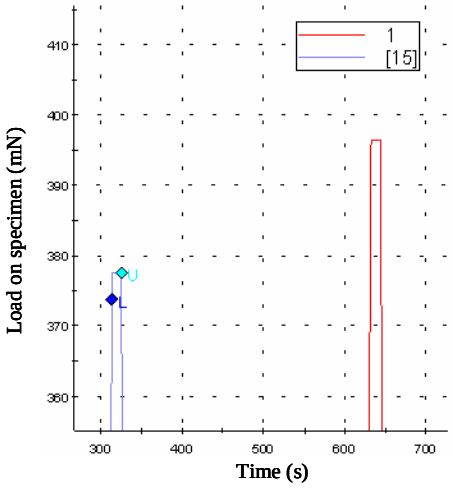


Figure (17). Load-time transient of the creep in the first and fifteenth cycles in anodic alumina film formed at 10 mA/cm² for 5400 s at 0 C˚

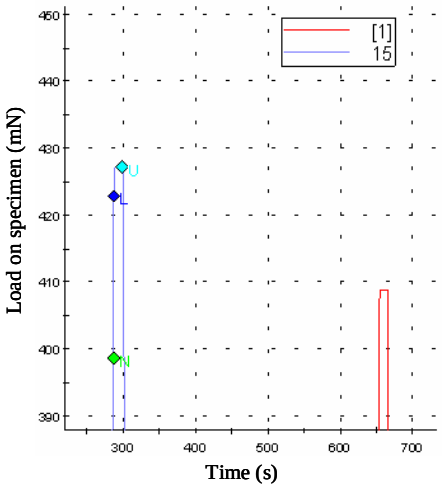


Figure (18). Load-time transient of the creep in the first and fifteenth cycles in anodic alumina film formed at 30 mA/cm² for 5400 s at 0 C˚

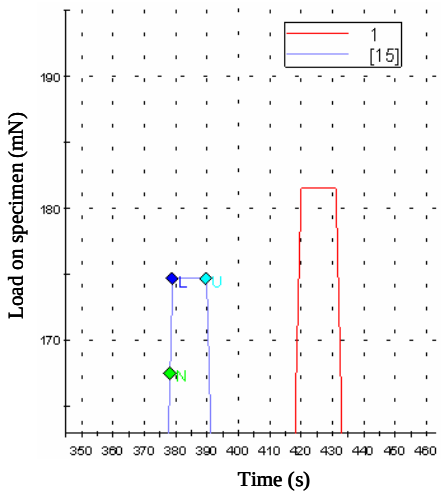


Figure (19). Load-time transient of the creep in the first and fifteenth cycles in anodic alumina film formed at 10 mA/cm² for 5400 s at 20 C˚

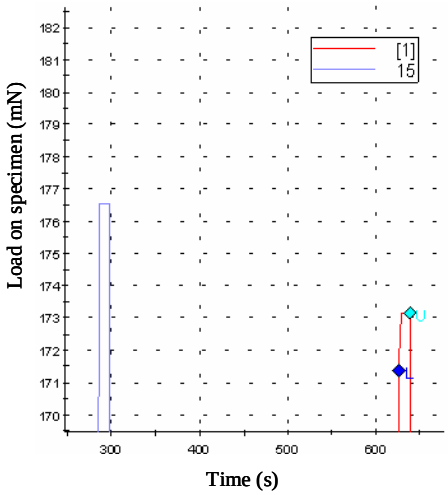


Figure (20). Load-time transient of the creep in the first and fifteenth cycles in anodic alumina film formed at 30 mA/cm² for 5400 s at 20 C˚

## 4. Discussion

The present study reports that the hardness of anodic alumina film decreases as the distance from aluminium substrate increases for whole films which completely agree with earlier results[41]. This reduction in hardness is due to the degradation of the film that caused by electrolyte attack, namely low hardness implies the existence of high degree of porosity and degradation in the film.

The rise of anodizing time and anodizing temperature leads to the increase in the reduction of hardness as result of an increase of degradation as revealed in previous findings[42]. The increase in porosity is caused by chemical dissolution of the film material during film growth.

This current study supports the previous findings[41] which reveal that the solubility of the film material in the anodizing electrolyte increases with rise of anodizing time and anodizing temperature. The current findings enhance the earlier work that suggests the increased porosity of the outer third of the film thickness might play significant role in low hardness and low elastic modulus in this region[41].

The hardness and elastic modulus rise with increase of current density for films fabricated at 20 C˚ in agreement with those of films grown in ammonium pentaborate[41] at 20 C˚. In contrast, the films formed at 0 C˚, the effect of current density is relatively small. This interprets that the degradation of the film is influenced by current density at high temperature but is not significant at low temperature. Low values of hardness and elastic at high temperature in current findings is compatible with previous results[41].

The effect of current density and anodizing temperature on the film thickness is determined by present work. It increases with rise of the anodizing current density and reduction in electrolyte temperature. This increase of the thickness is consistent with the rise in the anodizing voltage during steady film growth.

According to hardness measurements, films revealed an expected softening toward the film surface. The softening increases with rise of the anodizing time and temperature of electrolyte, which agrees with an increasing chemical degradation of the outer regions of the film by electrolyte.

## 5. Conclusion

Investigations of micro-hardness on cross-sections of the porous anodic films formed under various anodizing conditions. The hardness of the films was significantly dependent upon the depth within the oxide, decreasing with increased distance from aluminium/film interface. The reduction in the hardness is due to the chemical degradation that occurs in the outer region of the film during anodizing process, which increases as the anodizing temperature and anodizing time rise in range 0 to 20 C˚ and, 1000, 3000, 4000 and 5400 s respectively.

Nano-indentation of surface of anodic films grown at 10, 20 and 30 for 5400 s at 20 C˚ revealed that the hardness and elastic modulus rise linearly with increase of current density and reduction of anodizing time. In contrast, for hard films the values of both parameters are approximately constant, namely independent of the selected anodizing conditions, with respective values of about ~ 5.6 ± 0.40 GPa and ~ 110.8 ± 6 GPa. Reduction in hardness and elastic modulus with increased time for films formed at 20 C˚ implies that the chemical degradation is enhanced by increased temperature. The high values of the mean standard deviation of hardness and elastic modulus for films fabricated at 0 C˚ may be attributed to relatively high roughness and low homogeneity of the hard films and presence of flaws.

## References

[1] S. Ono, K. Asami, T. Osaka, N. Masuko, Structure of anodic films formed on magnesium, J. Electrochem. Soc. 143, L62 (1996).
[2] Capek D, Gigandet MP, Masmoudi M, Wery M, Banakh O. Long-time anodisation of titanium in sulphuric acid. Surf Coat Technol. 202(8):1379–84 (2008).
[3] Kumar S, Sankara N, Saravana K. Influence of fluoride ion on the electrochemical behavior of b-Ti alloy for dental implant application. Corros Sci. 52(5):1721–7. (2010).
[4] Neupane MP, Park IS, Lee SJ, Kim KA, Lee MH, Bae TS. Study of anodic oxide films of titanium fabricated by voltammetric technique in phosphate buffer media. J Electrochem Soc;4 (2):197–207 (2009).
[5] D. Gong, C.A. Grimes, O.K. Varghese, W. Hu, R.S. Singh, Z. Chen, E.C. Dickey, Titanium oxide nanotube arrays prepared by anodic oxidation, J. Mater. Res. 16 3331 (2001).
[6] R. Beranek, H. Hildebrand, P. Schmuki, Self-organized porous titanium oxide prepared in H2SO4/HF electrolytes, Electrochem. Solid-State Lett. 6 B12 (2003).
[7] J.M. Macak, P. Schmuki, Anodic growth of self-organized TiO2 nanotubes inviscous electrolytes, Electrochim. Acta 52 1258 (2006).
[8] V. Zwilling, M. Aucouturier, E. Darque-Ceretti, Anodic oxidation of titanium and TA6V alloy in chromic media: an electrochemical approach, Electrochim. Acta 45 921 (1999).

[9] H. Tsuchiya, J.M. Macak, I. Sieber, L. Taveira, A. Ghicov, K. Sirotna, P. Schmuki, Self-organized porousWO3 formed in NaF electrolytes, Electrochem. Commun. 7 295 (2005).
[10] H. Tsuchiya, J.M. Macak, I. Sieber, L. Taveira, P. Schmuki, Self-organized high- aspect-ratio nanoporous zirconium oxides prepared by electrochemical anodization, Small 1 722 (2005).
[11] F. Muratore, A. Baron-Wieche´ c, T. Hashimoto, P. Skeldon, G.E. Thompson, Anodic zirconia nanotubes: composition and growth mechanism, Electrochem. Commun. 12 1727 (2010).
[12] T.J. LaTempa, X. Feng, M. Paulose, C.A. Grimes, Temperature-dependent growth of self-assembled hematite (-Fe2O3) nanotube arrays: rapid electrochemical synthesis and photoelectrochemical properties, J. Phys. Chem. C 113 16293(2009).
[13] R.R. Rangaraju, A. Panday, K.S. Raja, M. Misra, Nanostructured anodic iron oxide filmas photoanode for water oxidation, J. Phys. D: Appl. Phys. 42 135303 (2009).
[14] T. Hashimoto∗, X. Zhang, X. Zhou, P. Skeldon, S.J. Haigh, G.E. Thompson Investigation of dealloying of S phase (Al2CuMg) in AA 2024-T3aluminium alloy, Corros Sci 103 157–164 (2016).
[15] F. Keller, M.S. Hunter, D.L. Robinson, Structural features of oxide coatings on aluminum, J. Electrochem. Soc. 100 411 (1953).
[16] J.P. O'Sullivan, G.C. Wood, The morphology and mechanism of formation of porous anodic films on aluminium, Proc. R. Soc. London, Ser. A 317 51 (1970).
[17] G.C. Wood, J.P. O'Sullivan, The anodizing of aluminium in sulphate solutions, Electrochim. Acta 15 1865 (1970).
[18] S. Wernick, R. Pinner, P.G. Sheasby, The Surface Treatment and Finishing of aluminium and Its Alloys, Finishing Publications Limited, Teddington, (1996).
[19] H. Masuda, K. Fukada, Ordered metal nanohole arrays made by a two-step replication of honeycomb structures of anodic alumina, Science 268 1466 (1995).
[20] H. Masuda, H. Yamada, M. Satoh, H. Asoh, M. Nakao, T. Tamamura, Highly ordered nanochannel-array architecture in anodic alumina, Appl. Phys. Lett. 71 2770 (1997)
[21] F. Li, L. Zhang, R.M.Metzger, On the growth of highly ordered pores in anodized aluminum oxide, Chem. Mater. 10 2470 (1998).
[22] K. Nielsch, J. Choi, K. Schwirn, R.B. Wehrspohn, U. Gösele, Self-ordering regimes of porous alumina: the 10% porosity rule, Nano Lett. 2 (7) 677 (2002).
[23] JP. Frayret, RP. Caprani, Anodic behaviour of titanium in acidic chloride containing media (HCl-NaCl). Influence of the constituents of the medium-I. Study of the stationary current. Calculation of the overall reaction orders. Electrochim Acta 26(12):1783–8 (1981).
[24] LT. Duarte, C. Bolfarini, SR. Biaggio, RC. Rocha-Filho, PA. Nascente, Growth of aluminum-free porous oxide layers on titanium and its alloys Ti–6Al–4V and Ti– 6Al–7Nb by micro-arc oxidation. Mater Sci Eng C 41(1):343–8 (2014).
[25] M. Fan, FL. Mantia, Effect of surface topography on the anodization of titanium. Electrochem Commun 37:91–5 (2013).
[26] G. El-Mahdy, KB. Kim, Monitoring the atmospheric corrosion loss of copper during wet/dry cyclic conditions in oxalic acid solutions. Corrosion 63(2):171–7 (2007).
[27] T. Ohtsuka, M. Masuda, N. Sato, Ellipsometric study of anodic oxide films on titanium in hydrochloric acid, sulfuric acid, and phosphate solution. J Electrochem Soc 132(4):787–92 (1985).

[28] D. Wang, H. Li, H. Yang, J. Ma, G. Li, Tribological evaluation of surface modified H13 tool steel in warm forming of Ti–6Al–4V titanium alloy sheet. Chin J Aeronaut 27(4):1002–9 (2014).
[29] P. Michal, A. Vagaská, M. Gombár, J. Kmec, E. Spišák, M. Badida, Prediction of the Effect of Chemical Composition of Electrolyte on the Thickness of Anodic Aluminium Oxide Layer. International Journal of Mathematical Models and Methods in Applied Sciences, vol 1, pp. 152-155 (2014).
[30] P. Michal, A. Vagaská, M. Gombár, A.Hošovský, J.Kmec, Monitoring of influence of significant parameters during anodizing of aluminium. In: 12th International Symposium on Applied Machine Intelligence and Informatics SAMI (2014), IEEE, Herľany, pp.49-54 (2014).
[31] J.R. Gregory, S.M. Spearing, Nanoindentation of neat and in situ polymers in polymer-matrix composites, Compos. Sci. Technol. 65 595e607 (2005).
[32] J. Rodríguez, M. Garrido-Maneiro, P. Poza, M. G_omez-del Río, Determination of mechanical properties of aluminium matrix composites constituents, Mater. Sci. Eng. A 437 (2006) 406e412, http://dx.doi.org/10.1016/ j.msea. 07.118 (2006).
[33] M. Hardiman, T.J. Vaughan, C.T. McCarthy, Fibrous composite matrix characterization using nanoindentation: the effect of fibre constraint and the evolution from bulk to in-situ matrix properties, Compos. Part A Appl. Sci. Manuf. 68 296e303 (2015).
[34] J.M. Kranenburg, C.A. Tweedie, K.J. van Vliet, U.S. Schubert, Challenges and progress in high-throughput screening of polymer mechanical properties by indentation, Adv. Mater. 21 3551e3561 (2009).
[35] J.A. King, D.R. Klimek, I. Miskioglu, G.M. Odegard, Mechanical properties of graphene nanoplatelet/epoxy composites, J. Appl. Polym. Sci. 128 4217e4223 (2013).
[36] R. De Silva, P. Pasbakhsh, K. Goh, S.-P. Chai, J. Chen, Synthesis and characterization of poly (lactic acid)/halloysite bionanocomposite films, J. Compos. Mater 48 3705e3717 (2014).
[37] T. Jin, X. Niu, G. Xiao, Z. Wang, Z. Zhou, G. Yuan, et al., Effects of experimental variables on pMMA nano-indentation measurements, Polym. Test. 41 37 (2015)
[38] W. Sautter, Aluminium, 42, 10, 636-42 (1966).
[39] G. M. Pharr Mater. Sci. Eng. A 253, 151 (1998).
[40] A. Bolshakov and G. M. Pharr J. Mater.Res. 13, 1049 (1998).
[41] A. German, Ph. D Thesis, University of Manchester (2002).
[42] G. E. Thompson and G. C. Wood, Anodic films on aluminium, Treatise onMaterials Science and Technology, Ed. By J. C. Scully, 23, 205 (1983).